Journal of Power Sources 196 (2011) 4411–4417

Contents lists available at ScienceDirect

Journal of Power Sources

journal homepage: www.elsevier.com/locate/jpowsour

Controllability study of an ethanol steam reforming process for hydrogen production

Vanesa M. García [a,*], Maria Serra [a], Jordi Llorca [b]

[a] Institut de Robòtica i Informàtica Industrial (CSIC-UPC), Llorens i Artigas 4-6, 08028 Barcelona, Spain
[b] Institut de Tècniques Energètiques, Universitat Politècnica de Catalunya (UPC), Diagonal 647, ed. ETSEIB, 08028 Barcelona, Spain

ARTICLE INFO

Article history:
Received 3 October 2010
Received in revised form 9 December 2010
Accepted 14 December 2010
Available online 24 December 2010

Keywords:
Steam reforming
Hydrogen production
Controllability
Control structures
MIMO system
PEMFC

ABSTRACT

A system for ethanol steam reforming and purification of carbon monoxide (CO) designed to feed a PEM fuel cell has been modelled. From the model, we study the sensitivity and controllability emphasizing the study of the influence of the temperature on the output variables of interest. The results of the study of controllability are used for the identification of the best control structures.

1. Introduction

The gradual reduction of fossil fuel reserves and the environmental pollution problems associated with their combustion have turned the attention of researchers to the search for alternative energy carriers. The energy vector that is currently receiving more attention is hydrogen, considered as a possible candidate to partially replace oil as fuel in mobile applications. However, hydrogen can only be considered a clean alternative if it comes from clean energy sources. Ethanol can be considered a source of H_2 neutral in relation to CO_2 emissions. This has motivated many investigations focusing on the design of reactors for the production of H_2, but less attention has been given to the control of the developed systems, that includes tasks such as the selection of the control structures and the design and tuning of the controllers. There exist different tools for the task of selecting the controlled, manipulated and measured variables and link these variables to make control loops [2]. The main mathematical methods for designing control structures are based on the relative gains [2] and singular value decomposition analysis [1,2]. In this work we select the most appropriate control structures for an ethanol reformer.

Reforming process

- Ethanol dehydrogenation to acetaldehyde and hydrogen (EtOHD)
- Acetaldehyde reforming (AcR)
- Water gas shift reaction (WGS)

Purification unit

- Condenser (CON)
- Preferential oxidation of CO (CO-PrOx)

2. Description of the ethanol steam reforming process and the dynamic model

In previous publications, we have described a non-linear dynamic model for a low-temperature ethanol steam reformer based on a cobalt catalyst [5]. It consists in a tubular reactor loaded with catalytic monoliths. The reforming process is divided in three separated stages (EtOHD, AcR and WGS). Experimental data for the kinetics of the two first stages was given in [3]. In this work, we have considered in addition a purification unit, which is required to directly provide hydrogen from the reactor to a fuel cell.

2.1. Description of the ethanol steam reforming process

2.1.1. Reforming unit

In the first stage, ethanol reacts over SnO_2 to produce acetaldehyde and hydrogen according to the reaction:

$$C_2H_5OH \rightarrow C_2H_4O + H_2 \quad (1)$$

* Corresponding author. Tel.: +34 93 401 58 05; fax: +34 93 401 57 50.
E-mail address: vgarcia@iri.upc.edu (V.M. García).

0378-7753/$ – see front matter © 2010 Elsevier B.V. All rights reserved.
doi:10.1016/j.jpowsour.2010.12.062

Nomenclature

C	concentration (mol m_R^{-3})
c_p	specific heat (J kg^{-1} K^{-1})
d_t	monolith external diameter (m)
F	molar flowrate (mol s^{-1})
k	reaction rate constant (mL g_{cat}^{-1} h^{-1})
K	equilibrium constant for homogeneous reaction
L	reactor length
t	time (min)
T	temperature (K)
T_F	furnace temperature (K)
U	overall heat-transfer coefficient (J s^{-1} m^{-2} k^{-1})
y	mole fraction
p	pressure (atm)
v	superficial velocity (m s^{-1})
x	conversion
r	velocity rate (mol m_R^{-3} s^{-1})
η^{H_2}	hydrogen yield (%)
OP	operating point

Subscripts

e	equilibrium
in	reactor input
out	reactor output
gas	gas
i	reaction number, $i = 1, \ldots, 3$ (ethanol decomposition, acetaldehyde reforming, water-gas shift, respectively)
j	component number, $j = 1, \ldots, 6$ (C_2H_5OH, H_2O, C_2H_4O, H_2, CO, CO_2, respectively)
C_2H_5OH	relative to ethanol
H_2O	relative to water
C_2H_4O	relative to acetaldehyde
H_2	relative to hydrogen
CO	relative to carbon monoxide
O_2	relative to oxygen
s	solid
S_1	stage 1
S_2	stage 2
S_3	stage 3

Greek letters

Δ	increment
υ_{ij}	stoichiometric coefficient of component j in reaction i
ρ	density (kg m^{-3})

The order of the reaction was established in [3] by changing the ethanol load at a series of temperatures between 573 and 673 K. A first-order reaction was identified and a kinetic law provided.

The acetaldehyde–steam mixture is transformed over Co(Fe)/ZnO catalyst in the second stage into a mixture of hydrogen, carbon monoxide, and carbon dioxide, according to the reactions:

$$C_2H_4O + H_2O \rightarrow 3H_2 + 2CO \quad (2)$$

$$C_2H_4O + H_2O \rightarrow 5H_2 + 2CO_2 \quad (3)$$

$$CO + H_2O \rightarrow CO_2 + H_2 \quad (4)$$

For the kinetics of reactions (2) and (3) a dependency on only acetaldehyde concentration was encountered [3]. The kinetics of the reaction (4) is based on the partial pressures of all the components involved in the reaction. The velocity rates of these reactions are:

$$r_{C_2H_4O} = k_{1,2}\, e^{E_{a,C_2H_4O}/RT} C_{C_2H_4O} \quad (5)$$

$$r_{CO,S2} = k_3\, e^{E_{a,CO}/RT} p_{CO}\, p_{H_2O} \left(1 - \frac{1}{K_{eq3}} \frac{p_{CO_2} p_{H_2}}{p_{CO} p_{H_2O}}\right) \quad (6)$$

The values of the reaction constants (k_1–k_3) are 1.38×10^4 mL g_{cat}^{-1} h^{-1}, 1.52×10^4 mL g_{cat}^{-1} h^{-1} and 9.2×10^2 mol m^{-3} s^{-1} atm^{-2}, respectively. The activation energies (E_{a,C_2H_4O}, $E_{a,CO}$) for these equations are 9.84×10^4 J mol^{-1} and 1.2×10^5 J mol^{-1}, respectively [3].

In the third stage, a Fe_2O_3–Cr_2O_3 catalyst has been used to further carry out the WGS for decreasing the CO content in the reformate. In this case, the experimental data are taken from [4]. This work has been chosen because it is based on operating conditions (rank of temperatures and pressure) similar to the conditions of our system. In this case, the Langmuir–Hinshelwood (L–H) model (7) describes adequately the reaction behaviour over the temperature and concentration ranges investigated [4].

$$r_{CO,S3} = k_{CO,S3}\, K_{CO}\, K_{H_2O} \left(\frac{p_{CO}\, p_{H_2O}\, (p_{CO_2}\, p_{H_2})/K_e}{1 + K_{CO}\, p_{CO} + K_{H_2O}\, p_{H_2O} + K_{H_2O} p_{H_2O}}\right) \quad (7)$$

2.2. Purification unit

The purification unit has been specifically included in this work and comprises a condenser and a CO preferential oxidation (CO-PrOx) reactor based on a Pt catalyst [6,7]. The condenser is used to cool hot vapors at the output of the third stage and separate hydrogen and carbon oxides from excess water and unreacted ethanol and acetaldehyde, whereas the purpose of the PrOx reactor is to reduce the concentration of CO at the inlet of the fuel cell stack. In the PrOx reactor, air is mixed with the feed stream to preferentially oxidize CO (8) while minimizing the consumption of H_2 (9):

$$CO + \frac{1}{2}O_2 \rightarrow CO_2 \quad (8)$$

$$H_2 + \frac{1}{2}O_2\, H_2O \quad (9)$$

As indicated in [7], the reaction rates in the CO-PrOx stage are described by:

$$r_{CO} = \frac{2k_{O_2} x_{O_2}}{\sqrt{x_{O_2}} + k_{CO}\sqrt{x_{O_2}}} \quad (10)$$

$$r_{H_2} = \frac{\sqrt{x_{H_2}}}{k_{CO}\sqrt{x_{CO}}} \frac{2k_{O_2} x_{O_2}}{\sqrt{x_{H_2}} + k_{CO}\sqrt{x_{CO}}} \quad (11)$$

$$2r_{O_2} = r_{CO} + r_{H_2} \quad (12)$$

where

$$k_{O_2} = 8.9 \times 10^6\, e^{10700/(RT_S)} \sqrt{\frac{P}{1.7}} \quad (13)$$

$$K_{CO} = 13.7 \quad (14)$$

To simulate the condenser, we have solved a system of non-linear equations with MATLAB™.

2.3. Dynamic model

To obtain the dynamic model of the system, pressure is considered constant at one atmosphere and the volumetric velocity variation along the reactor is taken into account.

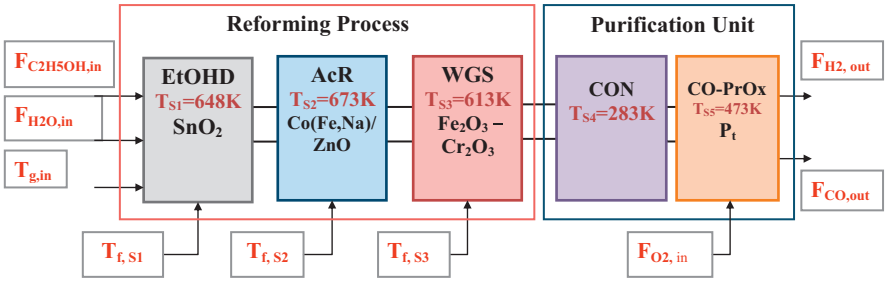

Fig. 1. Reforming and purification process of an ethanol–water mixture.

In the purification unit, isothermal conditions are assumed. Radial variations are neglected and only the axial profiles are considered.

The mathematical model is based on the mass balance and the energy balance, and it is assumed that the reactor is a pseudohomogeneous system by considering that the gas temperature and the solid temperature are the same [8].

Mass balance (for component j):

$$\frac{\partial C_j}{\partial t} + \frac{\partial v C_j}{\partial z} \upsilon_{j,i}\, r_i \tag{15}$$

Energy balance:

$$\rho_{\text{gas}}\, c_{p_{\text{gas}}} + \rho_s\, c_{p_s} \frac{\partial T}{\partial t} + \rho_g\, c_{p_{\text{gas}}} v \frac{\partial T}{\partial z} = \frac{4U}{d_t} T_F - T \Delta H_i r_i \tag{16}$$

The energy balance parameters [9] are $U = 4000\ [\text{J s}^{-1}\ \text{K}^{-1}\ \text{m}^{-3}]$, $\rho_s = 500\ [\text{kg m}^{-3}]$ and the density of the gas has been obtained from the following equation:

$$\delta_{\text{gas}} = \frac{\text{PM}_{\text{mi}}}{\text{RT}_{\text{gas,si}}} \tag{17}$$

To simulate the dynamic behaviour, initial conditions and boundary conditions are set as:

Initial conditions

$$\begin{aligned} &C_j(0,x) = C_{j0}(x) \quad \text{with} \quad x \in [1, L], j = 1, 2, \ldots 6 \\ &T(0,x) = T_0(x) \quad \text{with} \quad x \in [1, L] \end{aligned} \tag{18}$$

Boundary conditions

$$\begin{aligned} &C_j(t,0) = C_{je}(t) \quad \text{with} \quad t > 0 \\ &T(t,0) = T_e(t) \quad \text{with} \quad t > 0 \end{aligned} \tag{19}$$

The numerical solution of the partial differential equations (15) and (16) was accomplished by its transformation into an ODE-system by discretization of the spatial derivative. To this end, backward finite differences have been selected (first-order, 15 discretization points for the reported simulations) for the different stages of the reforming unit. The resulting 285 ODE equations were solved by an algorithm implemented in MATLAB™ (ODE45 Normand-Prince). Additional details regarding the mathematical model can be found in [5].

2.4. The linear model

A linearized model was obtained from the non-linear model of the system using SIMULINK® linearization tools, as reported in [3]. The state space representation of the system has a very large dimension and therefore, a model reduction strategy has been applied to transform the original model into a simplified form that has lower order and preserves the dynamic characteristics of the original high-order system [5]. The linear model is the base of the controllability study developed in this work. In addition, the comparison between the non-linear and the linear models will provide information about the suitability of selecting linear controllers. In this work, the goal is to perform a sensitivity and controllability analysis of the reforming process emphasizing the influence of the temperature variables. We have considered as inputs the flowrates of ethanol and water at the reactor entrance ($F_{C_2H_5OH}$, F_{H_2O}), the temperature of the entering mixture ($T_{g,in}$), and the temperatures of the furnaces of the three reforming stages ($T_{f,S1}$, $T_{f,S2}$, $T_{f,S3}$). As outputs (control objectives), we have selected the flowrates of H_2 and CO (F_{H_2} and F_{CO}) at the output of the reformer.

Fig. 1 shows the multiple inputs (manipulated variables) and multiple outputs (control variables) of the MIMO system.

The linear model in state space has the form:

$$\begin{aligned} x &= Ax + B_u u \\ z &= Cx + D_u u \end{aligned} \tag{20}$$

where the state x contains the concentrations of all components in the different volumes what the reactor has been divided. The input vector u contains the manipulated variables and the output vector z contains the controlled variables.

$$\begin{aligned} z &= [F_{H_2},\ F_{CO}] \\ u &= [F_{C_2H_5OH}\ F_{H_2O}\ T_{g,in}\ T_{f,S1}\ T_{f,S2}\ T_{f,S3}]^T \end{aligned} \tag{21}$$

2.5. Linear and non-linear models comparison

In this study, the nominal steady-state is selected at a H_2 yield value of $\eta^{H_2} = 80\%$ and a molar fraction of carbon monoxide of $y_{CO} = 0.83\%$ (see Table 3), which is suitable for entering the CO-PrOx reactor. The non-linear model is evaluated at four different operating points that correspond to the following variations with respect to the nominal operating point:

- OP_1 ($\Delta F_{C_2H_5OH}$): 10% ethanol input increase while the other five inputs are kept at the nominal values.
- OP_2 (ΔF_{H_2O}): 10% water input increase while the other five inputs are kept at the nominal values.
- OP_3 ($\Delta T_{g,in}$): 10% gas temperature input increase while the other five inputs are kept at the nominal values.
- OP_4 ($\Delta T_{f,S2}$): 5% furnace temperature of stage 2 input increase while the other five inputs are kept at the nominal values.

The response of F_{H_2} following step changes in the different inputs are shown in Fig. 2, where both, the linear and the non-linear model results have been plotted. It can be observed that the linear model curves have minimal differences with respect to the non-linear model curves in the case of changes in $F_{C_2H_5OH}$, F_{H_2O}, and $T_{g,in}$. On the contrary, the difference is notable when there is a change in $T_{f,S2}$. This non-linearity can complicate the control of the system if $T_{f,S2}$ is used as a manipulated variable to control F_{H_2}.

Fig. 3 shows the F_{CO} output response. The differences between the linear and non-linear models are small for step changes in the four considered inputs. The influence of $T_{f,S1}$ and $T_{f,S3}$ is not shown but has also been evaluated, and it has been seen that these temperatures cause more linear responses than $T_{f,S2}$. Therefore, from

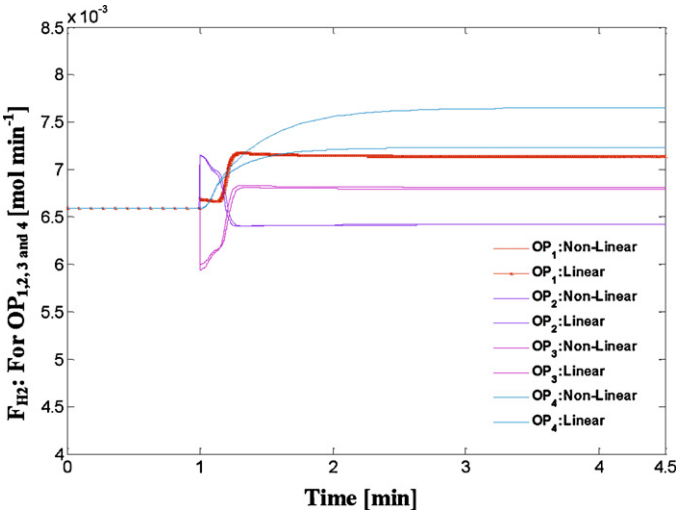

Fig. 2. Molar flow of hydrogen over time under incremental inputs in $F_{C_2H_5OH,in}$, $F_{H_2O,in}$, $T_{g,in}$ and $T_{f,S2}$.

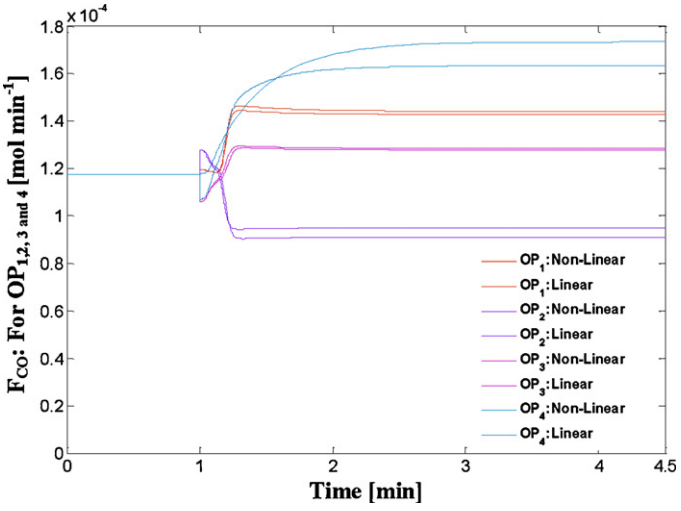

Fig. 3. Molar flow of carbon monoxide over time under incremental inputs in $F_{C_2H_5OH,in}$, $F_{H_2O,in}$, $T_{g,in}$ and $T_{f,S2}$.

this comparison of the linear and the non-linear models, it can be concluded that, although it will be important to take care of the influence of $T_{f,S2}$, the linear model can be considered a valid control analysis tool. The offsets between the linear model and the non-linear model profiles, are indicated numerically in Table 1.

2.6. Time evolution of the output variables due to input changes

The time evolution of the reforming process variables is critical because the fuel processor needs to regulate the amount of hydrogen provided to the fuel cell stack (anode) to avoid starvation or waste of hydrogen [10]. In Figs. 4–6, the resulting F_{H_2} and F_{CO} profiles at the output of stages 1, 2 and 3 are plotted. We have

Table 1
Gap between linearized systems at operating point.

Linearization points	Gap
OP_1	1.1×10^{-5}
OP_2	2.0×10^{-5}
OP_3	2.0×10^{-6}
OP_4	4.1×10^{-4}

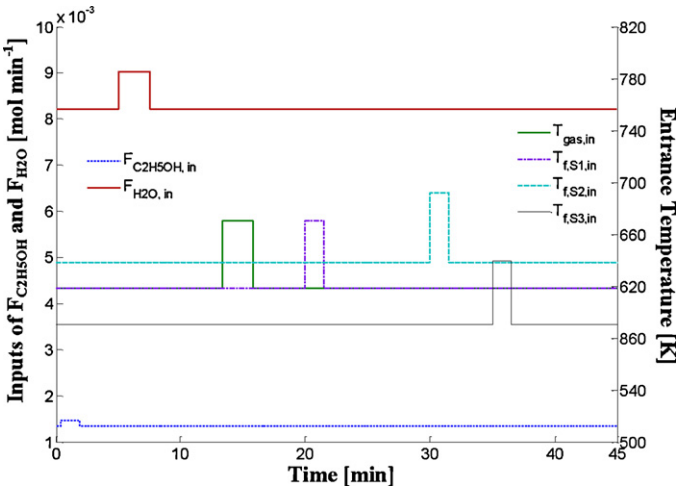

Fig. 4. Disturbances of the system, based on OP_n nominal conditions (see Table 2).

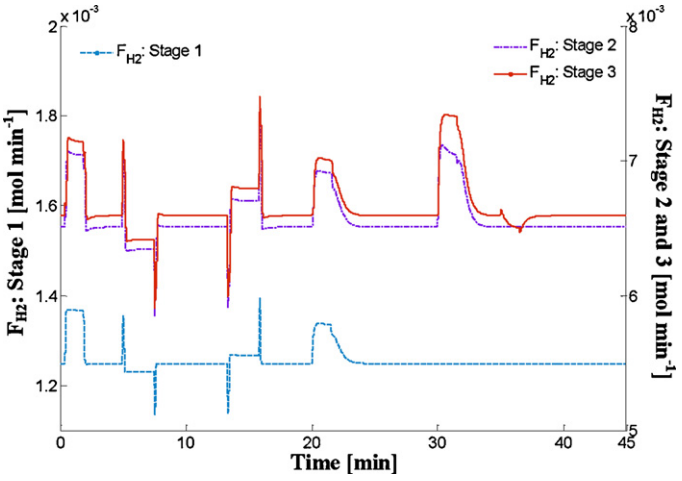

Fig. 5. Molar flow of hydrogen following the disturbances indicated in this figure.

excited the system by applying the disturbances represented in Fig. 4.

Fig. 5 shows hydrogen flows at the end of each one of the reforming process stages when disturbing the system as indicated in Fig. 4.

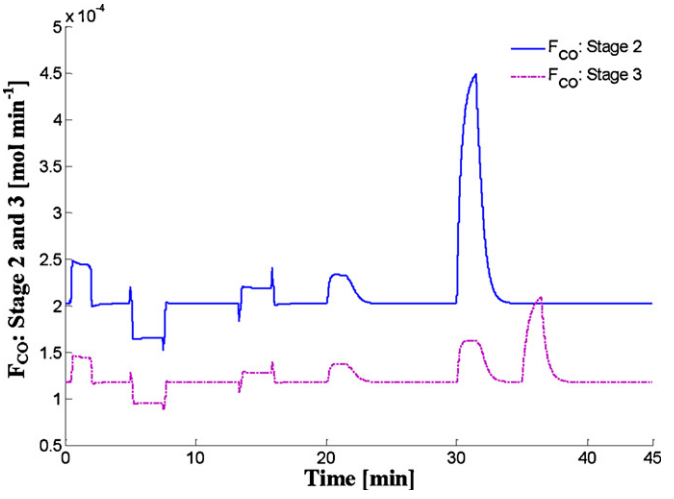

Fig. 6. Molar flow of carbon monoxide following the disturbances indicated in Fig 5.

Table 2
Input values at nominal operating point.

	$F_{C_2H_5OH,in}$ [$\times 10^{-3}$ mol/s]	$F_{H_2O,in}$ [$\times 10^{-3}$ mol/s]	$T_{g,in}$ [K]	$T_{f,S1}$ [K]	$T_{f,S2}$ [K]	$T_{f,S3}$ [K]
OP_n	1.34	8.21	648	648	673	633

High magnitude instantaneous peaks occur because the increase of the volume flow at the entrance of the reactor results in an immediate increase in the flow at the reactor exit. For $F_{C_2H_5OH}$ and T_{gas} disturbances, this peak is an inverse response. After these peaks, with a slower dynamics, the new F_{H_2} steady-state value is achieved. As expected, the time required to achieve the steady-state following variations in $F_{C_2H_5OH}$, T_{gas} and F_{H_2O} is less than that following disturbances in $T_{f,S1}$, $T_{f,S2}$ and $T_{f,S3}$. It is also relevant to notice that for $T_{f,S1}$ and $T_{f,S2}$, the time constant for positive changes is smaller than the time constant for negative changes. All these observations will be important at the controllers design stage. In Fig. 6 the behaviour of F_{CO} is shown, which is similar to that reported above for F_{H_2}. It is outstanding the influence of $T_{f,S2}$ at the exit of stage 2.

3. Steady-state sensitivity analysis

In accordance to Figs. 2 and 3, from a steady-state sensitivity analysis it is seen that an increase of 10% in $F_{C_2H_5OH}$ with respect to its nominal value originates an increase in F_{H_2} and F_{CO} at the outlet of stage 3 of 8% and 23%, respectively. Therefore, it is not appropriate to increase $F_{C_2H_5OH}$ when more F_{H_2} is required because larger quantities of F_{CO} will be produced as well. On the other hand, an increase of 10% in F_{H_2O} with respect to its nominal value produces a decrease in F_{H_2} and F_{CO} of 3% and 20%, respectively. Therefore, it can be said that the sensitivity of F_{CO} facing $F_{C_2H_5OH}$ and F_{H_2O} changes is higher than the sensitivity of F_{H_2}.

Concerning the effect of temperature, when the furnace temperature in zone 1 is increased in 10%, an increase in F_{H_2} and F_{CO} of 6% and 17%, respectively, takes place. When the furnace temperature in zone 3 is increased in 10%, an increase in F_{CO} of 37% and a reduction in F_{H_2} of 1.5% are observed. This is due to the water gas shift equilibrium, which yields CO at the expense of H_2 at high temperatures. This input variable is then very important as control variable because of the sensitivity of the system to produce excess CO when this temperature is changed.

Because of the special behaviour caused by changes in the furnace temperature of stage 2 found in the previous analysis, the sensitivity of the system in front of this variable is carefully considered. With this aim we have plotted the steady state values of the outputs flowrates (F_{H_2} and F_{CO}) following changes in $T_{f,S2}$ with respect to the nominal operating point (OP_n in Table 2).

In Figs. 7 and 8 the hydrogen yield, η^{H_2}, hydrogen molar flow rate, F_{H_2}, ethanol conversion, $x_{C_2H_5OH}$, and acetaldehyde conversion, $x_{C_2H_4O}$, are plotted at different $T_{f,S2}$ values. From Fig. 7 it is seen that an increase of the furnace temperature in stage 2 originates a slight increase in F_{H_2}, whereas η^{H_2} increases with a higher rate. According to the reaction scheme, acetaldehyde conversion ($x_{C_2H_4O}$) increases linearly with respect to temperature in stage 2 while the ethanol conversion ($x_{C_2H_5OH}$) is kept constant (Fig. 8). Fig. 9 shows F_{CO} at the outlet of stages 2 and 3. It can be seen that the influence of $T_{f,S2}$ over the CO production is very high.

4. Controllability study

In this section, a controllability analysis is performed using the Relative Gain Array (RGA), Condition Number (CN) and Morari Resiliency Index (MRI).

One of the most common approaches to control a multiple-input multiple-output (MIMO) system is to use a diagonal controller, which is often referred to as a decentralized controller. The decentralized control works well if the system is close to diagonal, which means that the plant can be considered as a collection of individual single-input single-output (SISO) subsystems that do not interact and can be considered independently. If an off-diagonal element is large, then the performance of the decentralized controller may be poor [2]. The controllability analysis based on RGA, CN and MRI permits to compare and select the control variables that minimise the interactions between crossed inputs and outputs.

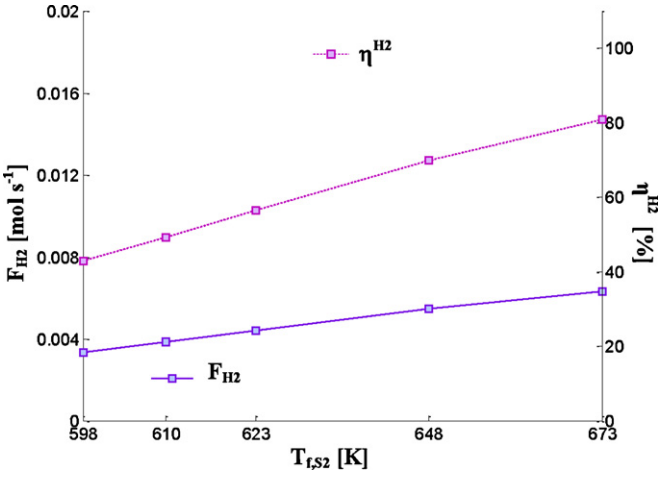

Fig. 7. Molar flow (solid lines) and yield of hydrogen (dotted lines) at different stage 2 furnace temperature values.

4.1. Relative Gain Array (RGA)

The Relative Gain Array is an analytical tool used to determine the optimal control structure of a MIMO system. The RGA is a normalized form of the gain matrix that describes the interactions between inputs and outputs. Through the RGA, the process interaction of open-loop and closed-loop control systems is measured for all possible input–output variable pairings. A ratio between open-loop gains to closed-loop gains are determined and the results are

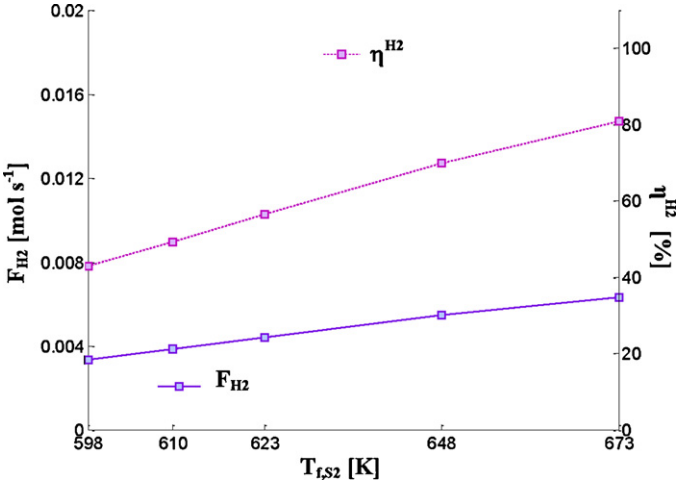

Fig. 8. Ethanol conversion (solid lines) and acetaldehyde conversion (dotted lines) at different stage 2 furnace temperature values.

Table 3
Output values at nominal operating point.

	$F_{H_2,out}$ [$\times 10^{-3}$ mol/s]	$F_{CO,out}$ [$\times 10^{-3}$ mol/s]	η^{H_2} [%]	$x_{C_2H_5OH}$ [%]	$x_{C_2H_4O}$ [%]	y_{CO} [%]
OP_n	6.39	1.34	79.7	93.4	84.5	0.83

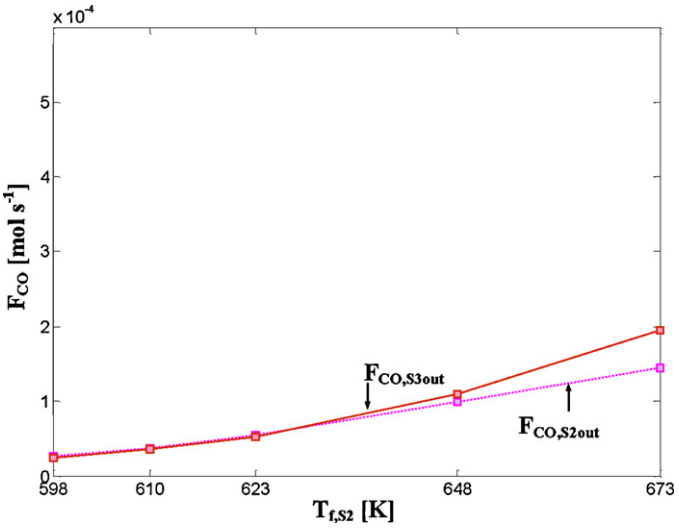

Fig. 9. Molar flow of CO as function of the incremental input $\Delta T_{f,S3}$ in the outlet of stages 2 and 3.

displayed in the RGA matrix. From the RGA analysis, different rules can be derived for the selection of the appropriate control variables and the best pairings between the selected inputs and the controlled outputs [2]. Basically, RGA matrixes close to the identity matrix are preferred and control structures with high RGA elements should be avoided.

To perform the analysis of controllability of the reforming process, all possible combinations of two inputs among the six possible inputs have been considered (Tables 3 and 4). The analysis is firstly done at zero frequency. At this frequency, pairs 1, 4, 8, 11 and 13 are the best because the values of RGA(1,1) are close to one. In contrast, pairs 6, 7 and 9 can be discarded because they have negative elements in the RGA at steady state. We also eliminated pairs 2, 3, 5, 10, 12 and 14 because with their high values in RGA(1,1), they would be very sensitive to input uncertainties.

4.2. Condition number (CN)

This index is the ratio between the maximum and minimum singular values of the gain matrix. High CN values indicate that it will be more difficult to control the process because of the sensitivity to uncertainties. For this reason we should select a set of inputs and outputs resulting in a system with small CN. Looking at CN values compiled in Table 4, pairs 1, 4, 8, 11 and 13 have the lower (preferred) values.

Table 4
Controllability index RGA, CN and MRI in $w = 0$ (rad/s).

PAIR	RGA(0)	CN(0)	MRI(0)
Pair 1: $F_{C_2H_5OH}$–F_{H_2O}	1.40	7.46	4.2×10^{-1}
Pair 2: $F_{C_2H_5OH}$–$T_{g,in}$	604	4.47×10^{-3}	1.2×10^{-3}
Pair 3: $F_{C_2H_5OH}$–$T_{f,S1}$	6.89	86.40	1.1×10^{-1}
Pair 4: $F_{C_2H_5OH}$–$T_{f,S2}$	9.5×10^{-1}	5.36	7.5×10^{-1}
Pair 5: $F_{C_2H_5OH}$–$T_{f,S3}$	11.50	92.11	2.65×10^{-2}
Pair 6: F_{H_2O}–$T_{g,in}$	-4×10^{-1}	9.66	0.53
Pair 7: F_{H_2O}–$T_{f,S1}$	-5.1×10^{-1}	120.65	7.8×10^{-2}
Pair 8: F_{H_2O}–$T_{f,S2}$	8.4×10^{-1}	15.95	2.56×10^{-1}
Pair 9: F_{H_2O}–$T_{f,S3}$	−0.48	15.95	2.56
Pair 10: $T_{g,in}$–$T_{f,S1}$	6.95	49.59	2.12×10^{-1}
Pair 11: $T_{g,in}$–$T_{f,S2}$	9.5×10^{-1}	5.16	1.1
Pair 12: $T_{g,in}$–$T_{f,S3}$	11.79	173.91	2.75×10^{-2}
Pair 13: $T_{f,S1}$–$T_{f,S2}$	9.4×10^{-1}	5.92	1.33
Pair 14: $T_{f,S1}$–$T_{f,S3}$	11.79	173.91	2.75×10^{-2}
Pair 15: $T_{f,S2}$–$T_{f,S3}$	5.66×10^{-2}	10.59	3.34×10^{-1}

4.3. Morari Resiliency Index (MRI)

The MRI (Morari Resilience Index) indicates whether a set of controlled variables and manipulated variables provides a simple control, giving a measure of the inherent controllability of the process: large values of MRI indicate that the process is more controllable. The pairs 1, 4, 8, 11 and 13 have also the higher MRI.

Having analysed the three controllability indexes at steady-state, it can be concluded that the control structures consisting in pairs 1, 4, 8, 11 and 13 are better than the other ones. For this reason, in the next section, only these structures will be considered.

5. Selection of the control structures

In this section, the steady state controllability analysis is completed with the analysis at different frequencies [2], and the best control structures are identified. Only pairs 1, 4, 8, 11 and 13 are taken into account. Pair 1 corresponds to of the manipulation of $F_{C_2H_5OH}$ for the control of F_{H_2}, and the manipulation of F_{H_2O} for the control of F_{CO}. On the other hand, for the pairs 4, 8, 11 and 13 if we need to control the F_{H_2} we should act on $F_{C_2H_5OH}$, F_{H_2O}, $T_{g,in}$ and $T_{f,S1}$, respectively. To control the F_{CO} we must act on the $T_{f,S2}$.

5.1. Controllability frequential analysis

The frequential analysis is done considering the frequency range from 10^{-3} to 10^{2} rad s^{-1}. In Figs. 10–12 the results obtained for the different controllability indexes are shown. In the three figures, the order of the different pairs is maintained during a wide frequency range. The peaks observed in the three figures are due to numerical problems and occur at different frequencies if the system model is trunked with a different number of states. Pairs 4, 11 and 13 are

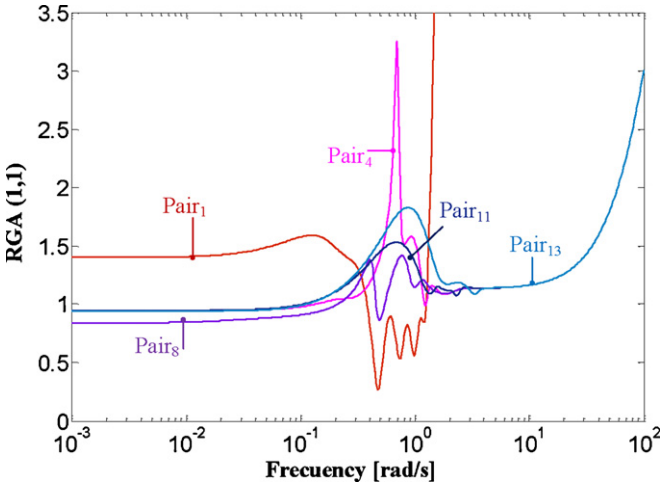

Fig. 10. Relative Gain Array RGA (1,1) of different pairs.

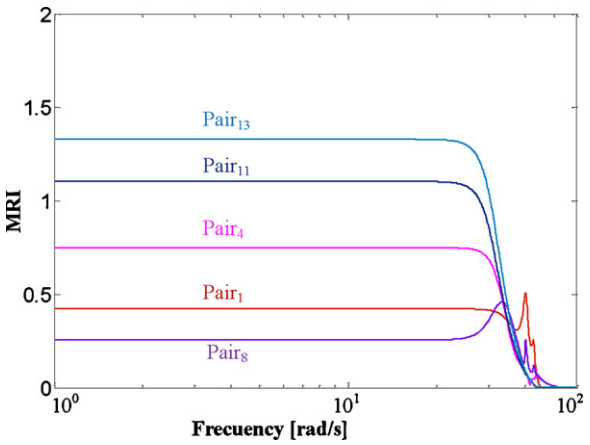

Fig. 11. Morari Resiliency Index (MRI) of different pairs.

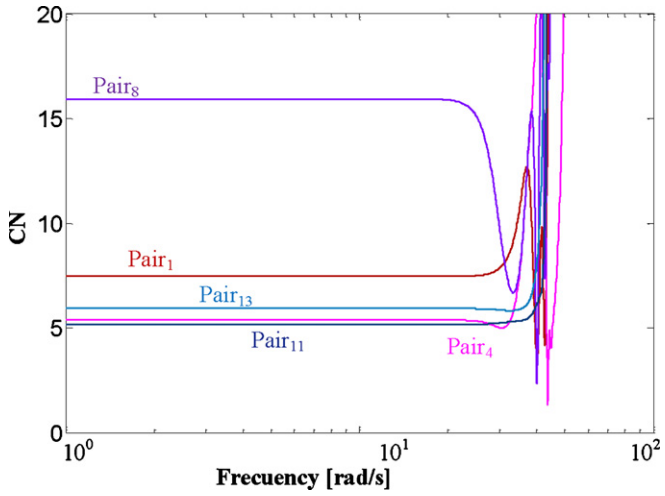

Fig. 12. Condition number (CN) of different pairs.

the best in accordance to the three controllability indexes. Their RGA(1,1) and MRI (close to one) and CN (lower than 10) are acceptable values for scaled systems. In the three cases, to control the F_{CO} the preferred manipulated variable is $T_{f,S2}$.

6. Conclusions

This work focuses on the design of controllers for an ethanol steam reformer, which is a MIMO system with six inputs and two controlled outputs. The main tasks of the work are the characterisation of the dynamic response and the selection of the preferred control structures. Both tasks are preliminary studies for the design of controllers. The dynamic response is analysed through a non-linear model. Inverse responses and non-linearities are observed. The controllability analysis is based on a linear model. In accordance to RGA, MRI and CN controllability indexes, three different control structures are selected as the most promising ones for the control of F_{H_2} and F_{CO}. They are the pairs consisting in the manipulation of $F_{C_2H_5OH}$ and $T_{f,S2}$, $T_{g,in}$ and $T_{f,S2}$, and $T_{f,S1}$ and $T_{f,S2}$. All three pairs include the $T_{f,S2}$. These control structures are a priori appropriate for 2×2 MIMO decentralised control. However, due to the non-linearities of the system, specially apparent in the $T_{f,S2}$ response, the performance of the controllers cannot be confirmed until its validation in non-linear models.

Acknowledgements

This work has been funded through MICINN projects DPI2010-15274 and CTQ2009-12520. V.G. is grateful to Generalitat de Catalunya for a PhD fellowship. J.L. is grateful to ICREA Academia program.

References

[1] E.H. Bristol, IEEE Trans. Automatic Control 55 (1966) 133–134.
[2] S Skogestad, I. Postlethwaite, Multivariable Feedback Control, second ed., Wiley, England, 2005.
[3] V. García, E. López, M. Serra, J. Llorca, J. Power Sources 192 (2009) 208–215.
[4] W. Poldolski, Y. Kim, Ind. Eng. Chem. 13 (1974) 415–421.
[5] V. García, E. López, M. Serra, J. Llorca, J. Riera, Int. J. Hydrogen Energy 35 (2010) 9768–9775.
[6] E. Bissett, Se. Oh, R. Sinkevitch, Chem. Eng. Sci. 60 (2005) 4709–4721.
[7] E. Bissett, Se. Oh, R. Sinkevitch, Chem. Eng. Sci. 60 (2005) 4722–4735.
[8] A. Cornelio, Indian Chem. Eng. 48 (2006) 164–174.
[9] A. Casanovas, M. Saint-Gerons, F. Griffon, J. Llorca, Int. J. Hydrogen Energy 33 (2008) 1827–1833.
[10] D. Megede, J. Power Source 106 (2002) 35–41.